

## Task 2: Corrosion Testing at 360°C

The autoclave corrosion tests for the model alloys were performed at both KAERI and Westinghouse. The testing environments at KAERI included both 360°C pure water and 360°C water containing 70 ppm Li while testing at Westinghouse was only in 360°C pure water. The testing in pure water was performed to assess the uniform corrosion behavior of the materials while testing in lithiated water was performed as an accelerated corrosion test and to assess the sensitivity of the alloys to lithium which is added to PWR coolant for pH control.

Autoclave testing was performed in accordance with ASTM G2 (Standard Test Method for Corrosion Testing of Products of Zirconium, Hafnium, and Their Alloys in Water at 680°F [360°C] or in Steam at 750°F [400°C]) in which the autoclaved is steamed prior to reaching the test temperature in order to reduce dissolved oxygen concentration.

Coupons were cut from the manufactured strip and measured approximately 25 mm × 20 mm × 0.8 mm in size. Duplicate samples from each alloy were tested to provide archive samples at intermediate exposure times. These samples were used for the oxide characterization task. The coupons were prepared for autoclaving by mechanically grinding the surface using 1200 grit SiC paper and then pickling in a solution of 5 vol.% HF, 45 vol.% HNO<sub>3</sub> and 50 vol.% H<sub>2</sub>O followed by thorough rinsing. The coupons were then measured and weighed prior to autoclaving.

The autoclave tests were performed to generate both pre-transition and post-transition corrosion data. The pre-transition data (specimen weight gain) were collected at relatively short time intervals during the first 50 to 100 days to characterize the pre-transition corrosion kinetics. Data collection at longer term intervals of about 30 days was performed to characterize the post-transition kinetics.

### *Westinghouse Test Results*

Westinghouse autoclave testing focused on the precipitate forming alloys as listed in Table 1.5. The materials included three alloy families (ZrFeCr, ZrCrFe, and ZrCuMo) along with reference material (Zircaloy-4 and Zr). The results for the 360°C water experiments are presented in the following series of figures, expressing measured weight gain in mg/dm<sup>2</sup> versus exposure time (days) for the model alloys. The results for the precipitate alloys show individual curves for several coupons of each alloy, whereas the particular samples archived for characterization are marked in red.

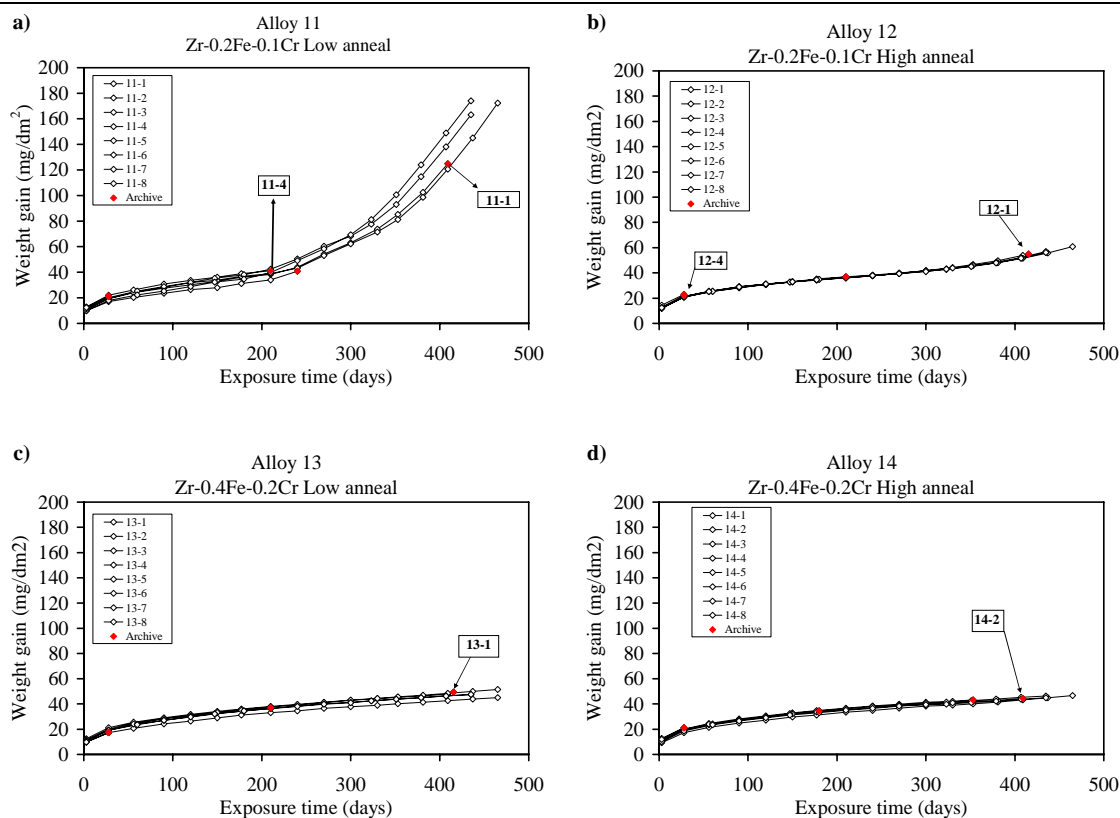
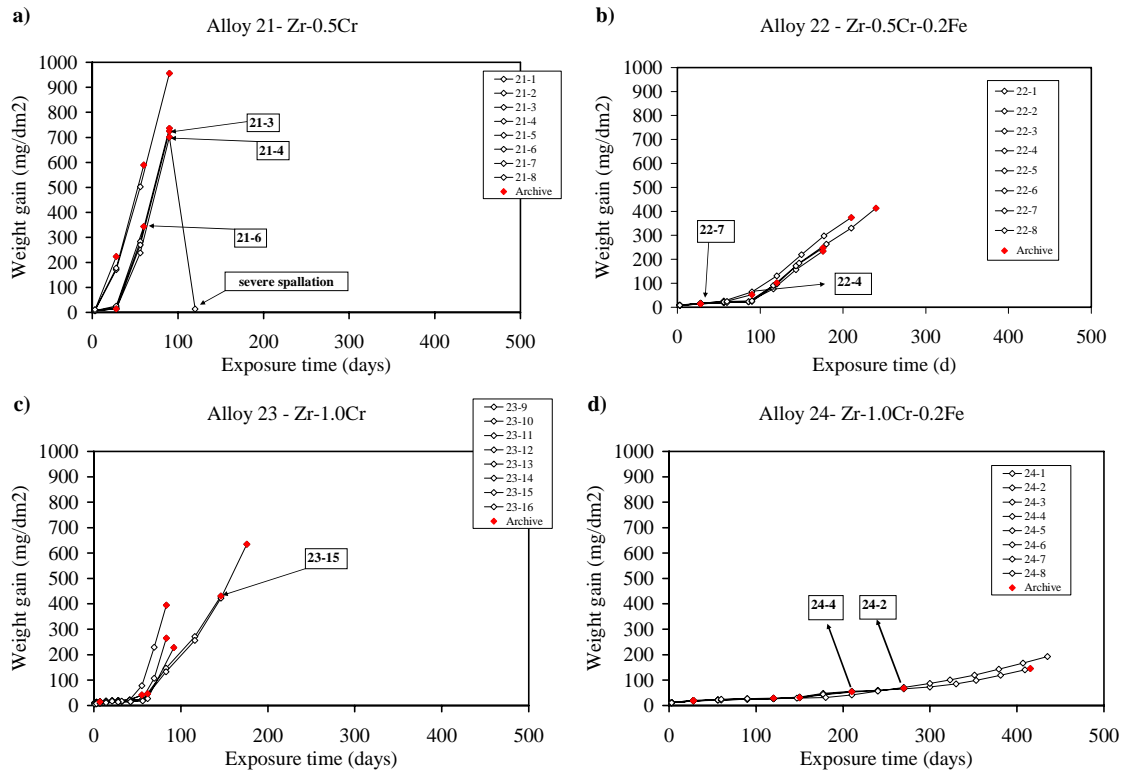


**Figure 2.1:** Weight gain *versus* time curves for the ZrFeCr alloy series after autoclave exposure to 360°C water at saturation pressure (18.7 MPa): a) Zr-0.2Fe-0.1Cr low temperature (580°C) anneal, b) Zr-0.2Fe-0.1Cr high temperature (720°C) anneal, c) Zr-0.4Fe-0.2Cr low temperature (580°C) anneal and d) Zr-0.4Fe-0.2Cr high temperature (720°C) anneal.

The weight gain curves for the ZrFeCr series (alloys 11-14) alloys are shown in Figure 2.1. The two alloys in this series had a constant Fe:Cr ratio = 2 (similar to Zircaloy-4) and were processed at 580°C or 720°C. The precipitate size increased with increased processing temperature and the volume fraction of precipitates increased as the Fe and Cr content increased.

Alloy 11 underwent breakaway at about 200 days of exposure. Alloy 12 shows signs of a transition or possible breakaway at around 300 days as the weight gain departs from a power law relationship. Alloys 13 and 14 had consistently the best corrosion resistance among the model alloys tested, suggesting that small additions of Fe and Cr up to 0.4 Fe (wt %) and 0.2 Cr (wt %) significantly enhance the corrosion resistance of Zr. These facts suggest that improvement in corrosion behavior is achieved with (i) an increase in the volume fraction of precipitates and (ii) an increase of precipitate size due to the fact that the same alloy (Zr-0.2Fe-0.1Cr) processed at a higher temperature survived with a protective oxide for a longer period of time (Alloy 12 versus Alloy 11).

The ZrCrFe alloys contain higher concentrations of Cr and Fe and were chosen for their potential application in high temperature environments. The precipitate chemistry in these alloys is different than the precipitate chemistry in the above ZrFeCr alloys due to the higher Cr content. Processing was performed at an intermediate temperature of 650°C.



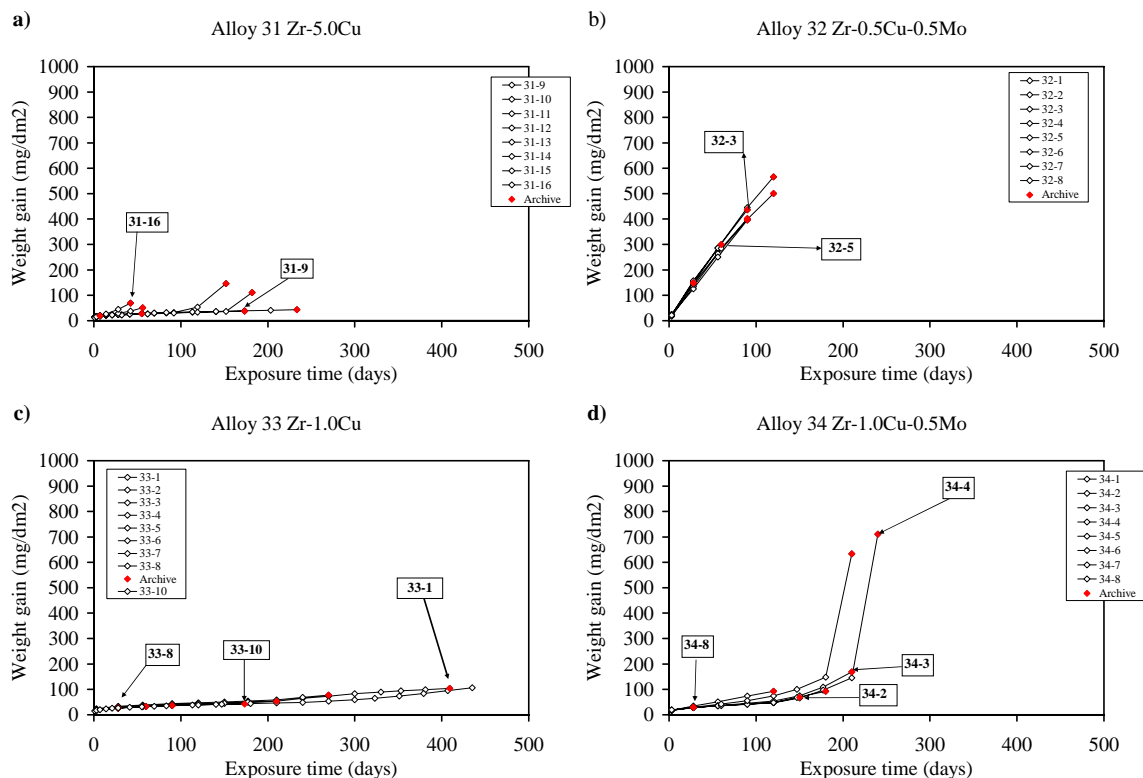
**Figure 2.2:** Weight gain *versus* time curves for the ZrCrFe alloy series after autoclave exposure to 360°C water at saturation pressure (18.7 MPa): **a)** Zr-0.5Cr, **b)** Zr-0.5Cr-0.2Fe, **c)** Zr-1.0Cr and **d)** Zr-1.0Cr-0.2Fe.

Figure 2.2 shows the weight gain curves for the ZrCrFe series (alloys 21-24). The Zr-0.5Cr and Zr-1.0Cr alloys did not exhibit good corrosion resistance, but some improvement was observed with the addition of 0.2 wt % Fe. The Zr-0.5Cr alloy suffered breakaway corrosion from the beginning of the testing while breakaway in the Zr-1.0Cr was delayed to about 50 days. The addition of 0.2 wt% Fe significantly increased the corrosion resistance of both of the Zr-Cr binary alloys. Zr-1.0Cr-0.2Fe exhibited the best corrosion resistance in this series and did not show signs of breakaway through the duration of test (~ 400 days).

The third set of alloys (ZrCuMo) was selected for their potential application at high temperature. The alloys also provided different precipitates than those present in ZrFeCr and ZrCrFe. Since Cu is a more noble metal than Fe and Cr, the susceptibility of Cu

containing precipitates to oxidation is expected to be lower and may have an impact on corrosion performance.

In the ZrCuMo alloys series (Alloys 31 to 34) the better performing alloys were the Zr-Cu alloys as shown in Figure 2.3. Alloy 31 (Zr-0.5Cu) has shown protective behavior for the duration of the test, but a few coupons did deviate from that behavior and have shown breakaway behavior. Alloy 33 (Zr-1.0Cu) consistently exhibited protective behavior up to 430 days, showing signs of a transition at about 200 days of exposure. Further exposure would be necessary to assess if the oxide would or not recover from the transition at 200 days, but the corrosion rate after the transition appears to be decreasing suggesting a transition rather than breakaway.



**Figure 2.3:** Weight gain *versus* time curves for the ZrCuMo alloy series after autoclave exposure to 360°C water at saturation pressure (18.7 MPa): **a)** Zr-0.5Cu, **b)** Zr-0.5Cu-0.5Mo, **c)** Zr-1.0Cu and **d)** Zr-1.0Cu-0.5Mo.

Commercially pure Zr (sponge and crystal bar) and Zircaloy-4 were also tested to serve as reference materials for the model alloys. Figure 2.4 shows the weight gain curves for the three reference alloys (Alloys 41-43).

The commercially pure Zr coupons either showed non protective behavior from the beginning of the corrosion test or in a few samples showed protective behavior up to 50 days of exposure. No significant differences were seen between Crystal bar and Sponge Zr, indicating that the higher impurity level of sponge Zr (~ 600 wt. ppm Fe versus 100 wt. ppm for crystal bar) did not impact corrosion behavior. After this period, a

destabilization of the oxide growth occurred that is characterized by a rapid acceleration of corrosion. After breakaway, the oxide turns white (characteristic of a porous, non-protective oxide) and powdery. This phenomenon is termed “breakaway corrosion” and is distinguished from an oxide transition which recovers stable growth.

---

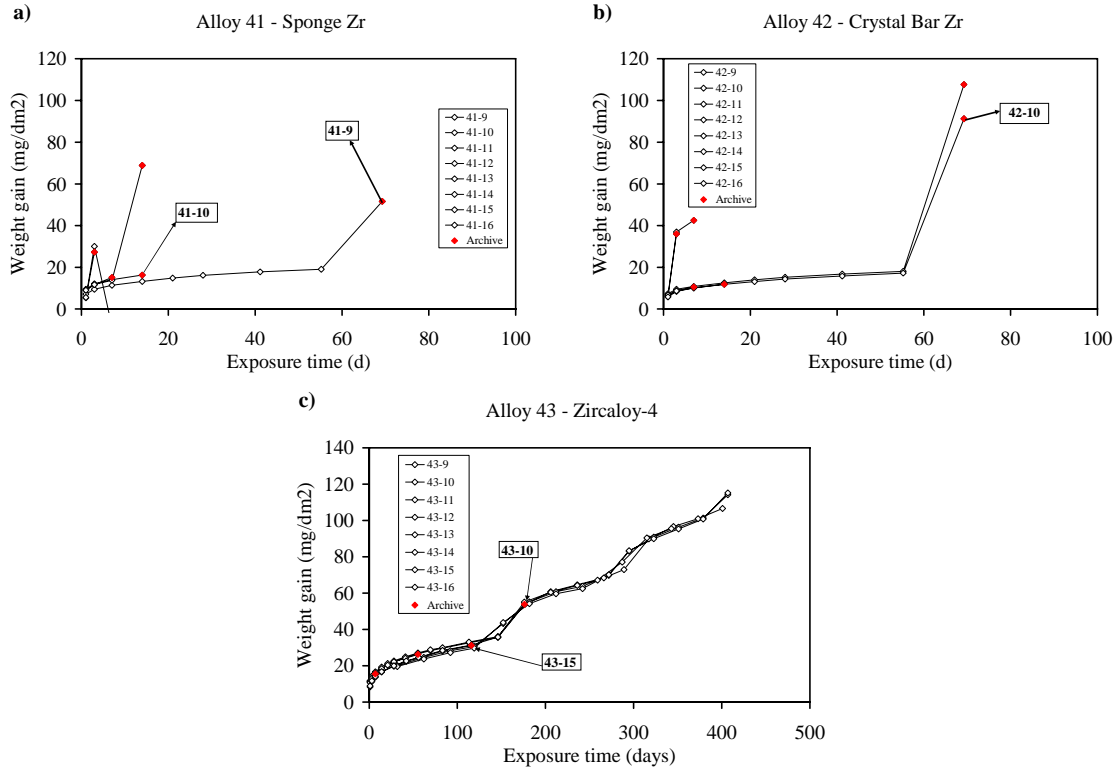


**Figure 2.4:** Weight gain *versus* time curves for the ZrCrFe alloy series after autoclave exposure to 360°C water at saturation pressure (18.7 MPa): **a)** Sponge Zr **b)** Crystal Bar Zr and **c)** Zircaloy-4.

---

The weight gain observed for Zircaloy-4, manufactured in the same way as the model alloys, is shown in Figure 2.4c. The Zircaloy-4 samples exhibit the classical behavior of cyclic oxide growth. After approximately 150 days there is an increase in the corrosion rate, associated with the temporary loss of protectiveness at the oxide transition, followed by the reconstruction of the protective oxide and the re-establishment of the same kinetics exhibited before the transition. The oxide growth is stable and the appearance of the oxide is black and shiny.

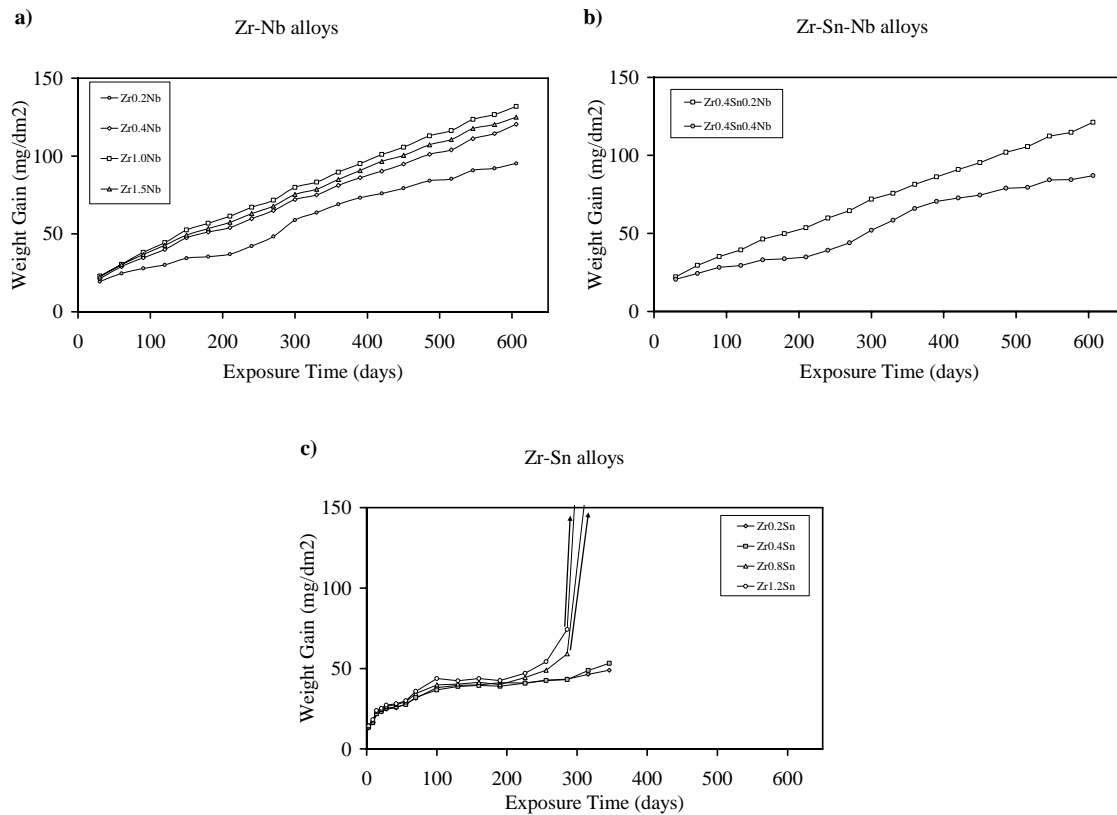


**Figure 2.5:** Weight gain *versus* time curves for the ZrNb, ZrSn and ZrNbSn alloy series after autoclave exposure to 360°C water at saturation pressure (18.7 MPa): **a)** ZrNb **b)** ZrNbSn and **c)** ZrSn.

Figure 2.5 shows the weigh gains curves for the model solid solution alloys (ZrNb, ZrSn and ZrNbSn) that were investigated in this project. The ZrSn alloys exhibit higher initial corrosion rates and an oxide transition around 50-60 days of exposure. It is also clear that some weight loss occurs after 120 days, likely due to oxide spalling. The higher Sn content alloys (0.8 and 1.2 wt%) suffered unstable oxide growth after 280 days of exposure. The lower Sn content alloys resisted and formed protective oxide layers up to the duration of the test, about 350 days. A second transition seems to be taking place at 300 days, but further data would be necessary to access that possibility. The increase in corrosion rate at 300 days may lead to unstable growth of oxide, i.e., breakaway corrosion.

In the ZrNb system, the Zr-0.2Nb alloy showed lowest corrosion with little dependence of corrosion rate with Nb content between 0.4 and 1.5 Nb. No clearly marked transition in corrosion kinetics was observed in the ZrNb alloys.

The ZrNbSn alloys showed an oxide transition but exhibited corrosion rates that were similar to the equivalent Zr-Nb alloys of the same Nb content.

Figure 2.6 shows images of the autoclaved coupons exposed to 360°C water. As seen in the images, the oxides formed on different alloys have different characteristics. The oxide formed on alloy 14 (Zr-0.4Fe-0.2Cr, 720°C) is intact and shiny black, as were all the oxides formed on the ZrFeCr model alloys. The oxide formed on alloy 21 (Zr-0.5Cr) has a green color due to presence of Cr. Although the alloy has undergone breakaway corrosion, no spallation of the oxide occurred. Oxides formed on the remaining ZrCrFe alloys presented similar aspects, even after breakaway. The oxide formed on alloy 33 (Zr-1.5Cu) is also intact as opposed to the oxide formed on alloy 34 (Zr-1.0Cu-0.5Mo) where the oxide is in the process of losing its integrity and pieces of oxide spalling from the surface of the sample. The oxide formed on the Crystal Bar Zr is different from the ones formed on the other alloys. As shown in Figure 2.6, the oxide is initially black and then begins to turn into a white and powdery oxide with exposure time; the final oxide, which is also a breakaway oxide, is completely powdered and white.

The results suggest that the alloy composition and microstructure play a dominant in determining corrosion behavior. Minor changes in the composition of the alloys can lead to dramatic changes in corrosion behavior, as, for example, the addition of 0.2Nb to pure Zr.

In general, the best performing alloys in water 360°C were from the ZrFeCr system and the best behaving alloy was alloy 14, Zr-0.4Fe-0.2Cr, 720°C. This is in accordance to Barberis *et al*, where they found that in addition to the second phase particle (SPP) size, their volume fraction is an important parameter. An increase in volume fraction of the SPPs would decrease the corrosion rate, whatever nature of the SPP. Alloy 14 has the highest SPP volume fraction among the ZrFeCr model alloys.

The key to good corrosion resistance is to avoid breakaway corrosion and to maintain a stable, protective oxide and oxide growth. The pre-transition portion of the weight gain curves were systematically fit to the power law of the type  $W = K t^n$ , where  $W$  is weight gain,  $K$  is the pre-exponential and  $t$  is time. The pre-exponential term  $K$  is a rate at which the sample gains weight per unit of time to the power of  $n$ . Characterization of the oxidation kinetics was performed based upon three factors:  $K$ ,  $n$ , and time to transition.

The fit to the corrosion data was performed on the average weight gain measurement from 4-8 samples. The power law used to fit the curves provided an excellent fit to the corrosion results ( $R^2$  values were consistently near 0.99). The weight gains of the individual samples were also fit with the same power law, and very similar values of  $A$  and  $n$  were obtained. This shows that the results are consistent from sample to sample and there is little variability in the corrosion results, more specifically in the pre-transition regime.

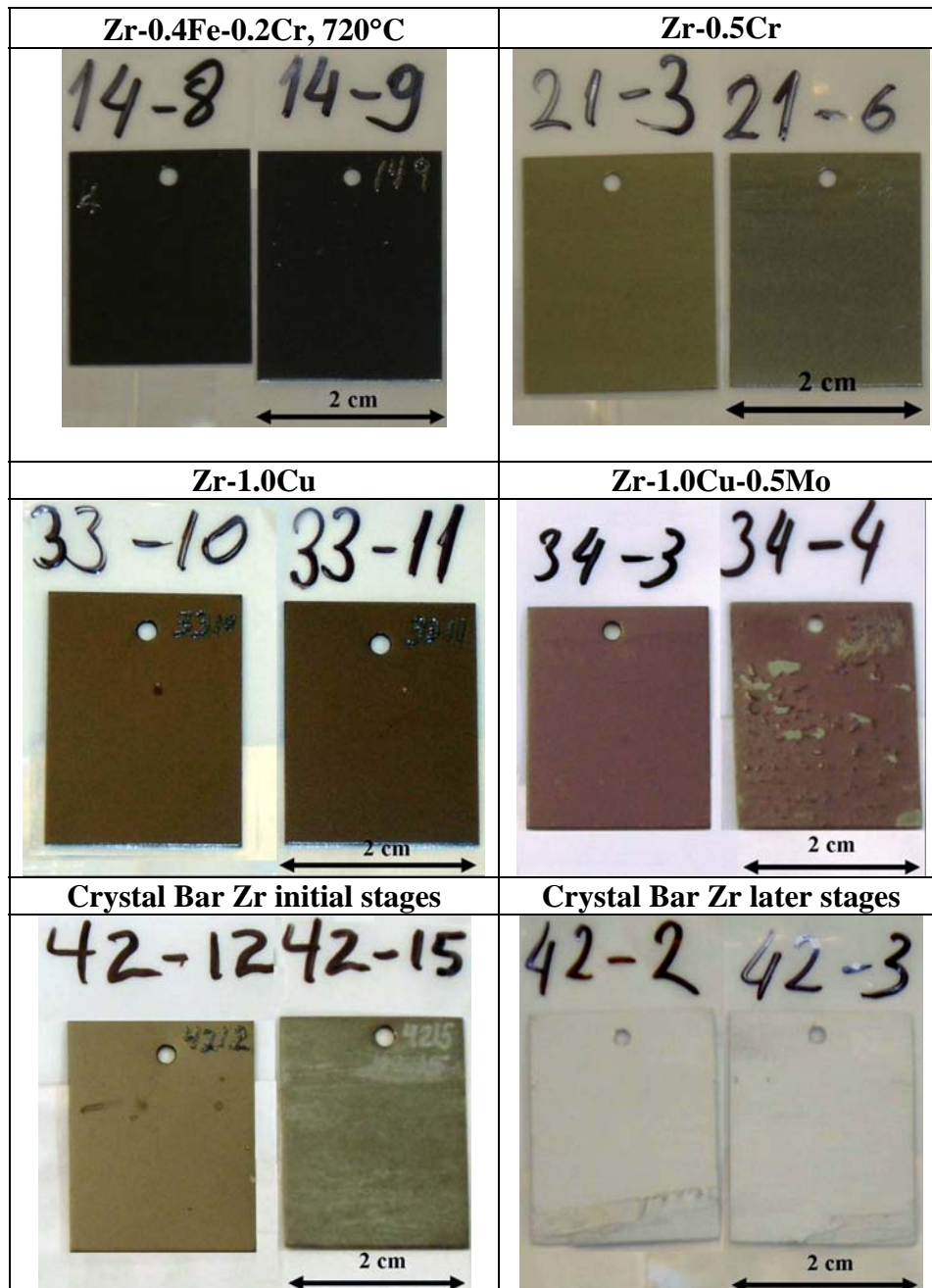
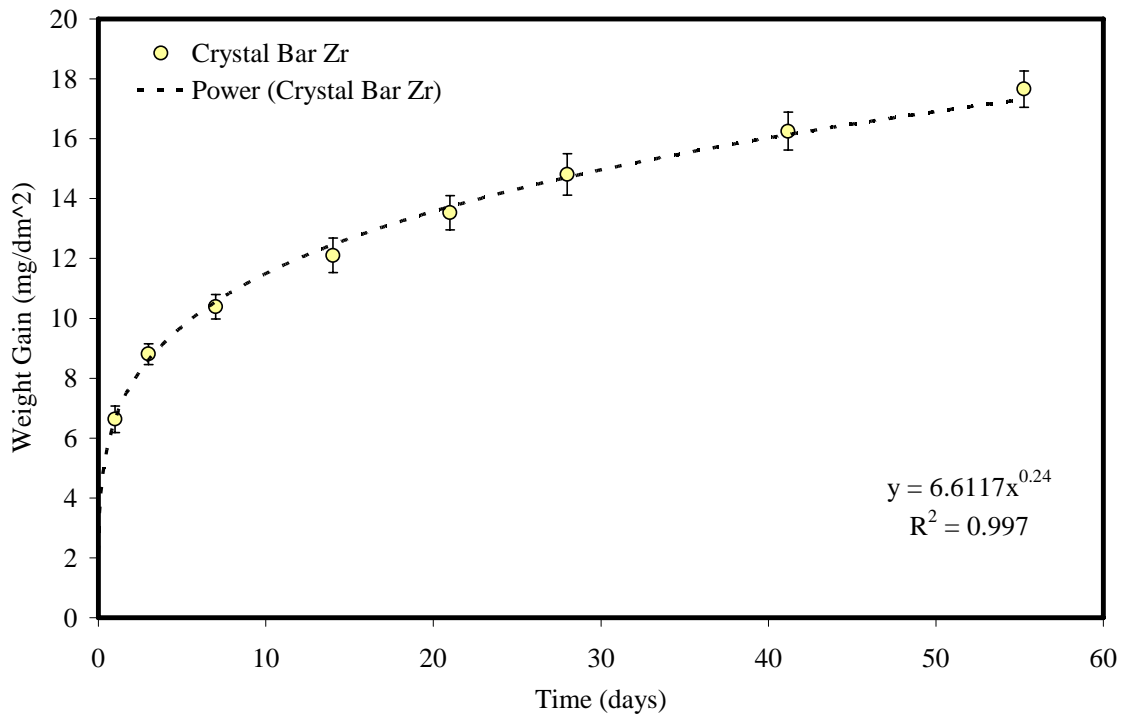


Figure 2.6: Zr alloy coupons autoclaved in 360°C water.



**Figure 2.7:** Fit of the weight gain *versus* exposure time curve to the power law of the type  $W = A.t^n$ , for Sponge Zr. The points represent averages of the samples 42-09, 42-10, 42-11 and 42-12 in 360°C water.

Figure 2.7 shows an example of the fit of the weigh gain curve for Zr sponge (Alloy 42). The constants for the fitted curves for the pre-transition kinetics of the model alloys in water 360°C are tabulated in Table 2.1.

The calculated values of  $n$  are almost all below 0.5, and some significantly below (~0.18), indicating in most of the alloys a significant deviation from a pure diffusion based process and consequent parabolic behavior. The reason for these departures is not clear, but could be related to factors in the oxide that hamper or impede diffusion. These could include the presence of lateral cracks which serve as obstacles to oxygen ion migration, increasing grain size within the oxide could reduce grain boundary diffusion, or the presence of stress, all of which could slow down diffusion and affect the value of  $n$ . Another possibility is related to the fact that the protective layer of the oxide is only a fraction of the measured oxide layer; if this fraction changes (increases) with thickness then kinetics lower than parabolic could be established. Finally, it is possible that slower electron transport through the oxide layer slows down oxygen ion transport.

It is important to notice that the values of  $n$  shown in Table 2.1 are characteristic of each alloy series. The ZrNb samples have an average  $n$  of 0.42, reasonably close to parabolic. In the Zr-Sn alloys, the average  $n$  is 0.32 and for ZrNbSn it is 0.41. In contrast to the precipitate forming alloys, including Zircaloy-4, the value of  $n$  is closer to 0.2.

In comparing Zircaloy-4 with the model alloys made from its individual constituents (Sn, Fe, Cr), it is possible to observe that an alloy with the same FeCr content as Zircaloy behaves quite well, and does not show an oxide transition within the time tested (Zr-0.4Fe-0.2Cr). At the same time the ZrSn alloys show a transition and subsequently, breakaway (Zr-0.8 and 1.2 Sn).

Table 2.1: Pre-transition kinetics constants for model Zr alloys test in the 360°C water.

<i>Alloy Group</i>	<i>Alloy</i>	<i>A</i>	<i>n</i>	<i>ave. A</i>	<i>ave. n</i>
Zr-Fe-Cr	Zr-0.2Fe-0.1Cr, 580°C	10.2	0.20	9.89	0.21
	Zr-0.2Fe-0.1Cr, 720°C	10.2	0.20		
	Zr-0.4Fe-0.2Cr, 580°C	9.78	0.21		
	Zr-0.4Fe-0.2Cr, 720°C	9.39	0.22		
Zr-Cr-Fe	Zr-0.5Cr	non-protective from the beginning of test		10.9	0.19
	Zr-0.5Cr-0.2Fe	11.5	0.17		
	Zr-1.0Cr	9.73	0.21		
	Zr-1.0Cr-0.2Fe	11.6	0.18		
Zr-Cu-Mo	Zr-0.5Cu	13.6	0.17	14.1	0.18
	Zr-0.5Cu-0.5Mo	13.6	0.17		
	Zr-1.0Cu	15.1	0.17		
	Zr-1.0Cu-0.5Mo	14.0	0.21		
Zr	Sponge Zr	8.50	0.20	7.56	0.22
	Crystal Bar Zr	6.61	0.24		
Zircaloy	Zircaloy-4	11.0	0.21	10.20	0.22
	Zr-4 Control	9.40	0.23		
Zr-Sn	Zr-0.2Sn	9.30	0.29	9.50	0.29
	Zr-0.4Sn	8.10	0.32		
	Zr-0.8Sn	10.0	0.27		
	Zr-1.2Sn	10.6	0.27		
Zr-Sn-Nb	Zr-0.4Sn-0.2Nb	5.92	0.43	6.52	0.41
	Zr-0.4Sn-0.4Nb	7.11	0.39		
Zr-Nb	Zr-0.2Nb	6.40	0.43	5.92	0.45
	Zr-0.4Nb	5.00	0.52		
	Zr-1.0Nb	5.90	0.45		
	Zr-1.5Nb	5.80	0.44		
	Zr-2.5Nb	6.50	0.40		

### *KAERI Test Results*

Parallel corrosion testing was also performed at KAERI. The autoclave corrosion tests for the model alloys included testing in both 360°C pure water and in 360°C lithiated water.

Zr-Fe-Cr alloy, which was manufactured by US and transferred to ROK, was tested in 360°C water and in 360°C lithiated water using the autoclaves in KAERI. Zr-Fe-Cr alloys were designed to change the size and the volume fraction of the precipitates by varying the alloying element content and the processing temperature. Figure 2.8 shows the corrosion behavior of Zr-Fe-Cr alloys in 360°C water as well as in 360°C lithiated water. Zr-0.2Fe-0.1Cr and Zr-0.4Fe-0.2Fe which were manufactured by the higher temperature processing (720°C) showed a lower corrosion rate. However, the breakaway behavior was observed in the alloys processed at the lower temperature (580°C). Some part of the oxide, especially in the vicinity of the edges showed the evidence of the corrosion acceleration, but the remaining part of the oxide still showed a black color and an adherent behavior. Such a localized corrosion behavior seems to result from the inhomogeneity of the base alloy rather than a specific corrosion behavior. This non-uniform corrosion behavior was not in the Zr-0.4Fe-0.2Cr (580°C) material tested in the US and may be a result of variability in individual coupons. Zr-Fe-Cr alloys showed the breakaway behavior at around 150 days in lithiated water except for Zr-0.4Fe-0.2Cr(H) that maintained lower corrosion rate and a black, adherent oxide up to 450 days. The excellent behavior of Zr-0.4Fe-0.2Cr (H) was consistent with the US results.

The corrosion behavior of Zr-Cr and Zr-Cr-Fe alloys, which were manufactured in the US and transferred to ROK, was evaluated in 360°C water and in 360°C lithiated water. Figure 2.9 shows the corrosion behavior of Zr-Cr and Zr-Cr-Fe alloys. Zr-0.5Cr and Zr-1.0Cr showed a higher corrosion rate and have the brown-colored oxide. The corrosion rate of both binary Zr-Cr alloys was poor with the rate of Zr-0.5Cr being higher than that of Zr-1.0Cr. The results were similar to those observed in the US testing with poor corrosion of both binary Zr-Cr alloys. On the other hand, Fe-containing alloys showed a low corrosion rates and have a black-colored oxide up to 430 days. The corrosion rate of the two Fe-containing alloys was almost the same as each other. It was confirmed that the beneficial effect of Fe was explicit. Testing in the US also showed the beneficial effect of Fe in the Zr-1.0Cr-0.2Fe alloy. In lithiated water, however, all the alloys showed the breakaway behavior after 90 days except for Zr-0.5Cr-0.2Fe alloys where the breakaway was occurred at 140 days.

Zr-Cr and Zr-Cr-Fe was also manufactured in ROK with the same nominal composition and the same manufacturing process and tested along with US-manufactured Zr-Cr and Zr-Cr-Fe alloys. Their corrosion behavior in 360°C pure and in lithiated water was depicted in Figure 2.10. The corrosion behavior of ROK-manufactured Zr-Cr-Fe alloys was almost similar to the US-manufactured Zr-Cr-Fe alloys. Fe-containing alloys maintained low corrosion rate up to 600 days and have a black and adherent oxide. In

lithiated water, all the Zr-Cr-Fe alloys showed the breakaway behavior after 60 days. However, the weight gain increment of Fe-containing alloys was smaller when compared to Zr-Cr alloys. The beneficial effect of Fe was also confirmed to be clear even in the lithiated water.

The US-manufactured Zr-Cu-Mo alloys showed the breakaway behavior at the early stage of the corrosion test and the oxide turned white as shown in Figure 2.11. The Zr-Cu alloys survived to more than 400 days and retained a black, adherent oxide. The addition of Cu was shown to be deleterious in lithiated water: Zr-1.0Cu and Zr-1.0Cu-0.5Mo showed the breakaway behavior just after 60 days whereas the time to transition was extended to 180 days in Zr-0.5Cu and Zr-0.5Cu-0.5Mo which showed the trace of the localized corrosion on the oxide surface.

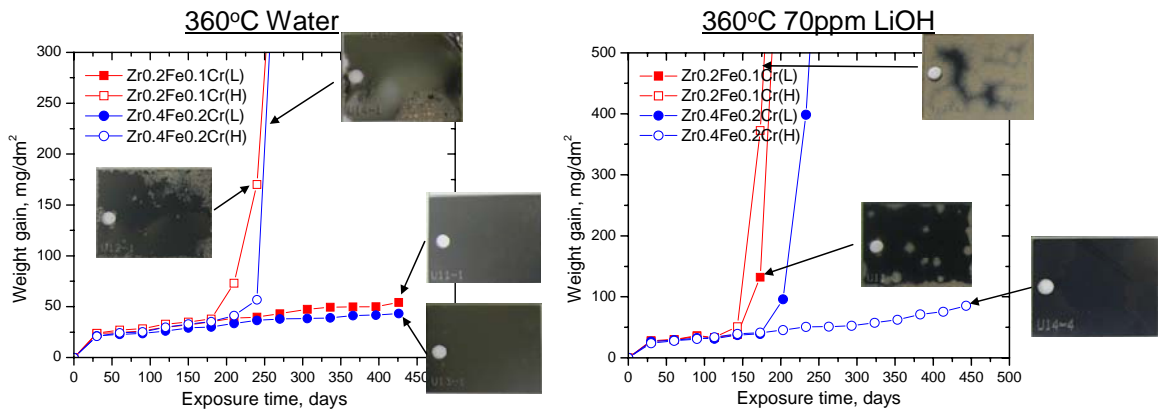
Figure 2.12 shows the corrosion test result for the ROK-manufactured Zr-Cu-Mo alloys. The corrosion resistance of ROK-manufactured Zr-Cu-Mo alloys showed the breakaway behavior except for Zr-1.0Cu alloys which have a low corrosion rate and a black oxide up to more than 600 days. The alloys with a higher Cu content showed a better corrosion resistance. The breakaway occurred at the earlier time in the Mo-containing alloy. The results are qualitatively similar to the corrosion results from the testing in the US with the Zr-Cu binary alloys exhibiting better behavior than the Mo-bearing alloys. In lithiated water, all the Zr-Cu-Mo alloys showed the breakaway behavior at the early stage of the corrosion test.

Corrosion tests were also performed for the reference alloys: Zr sponge, crystal bar Zr and Zircaloy-4 which were supplied by the US. Figure 2.13 shows the corrosion behavior of the reference alloys in 360°C water and in 360°C lithiated water. The sponge Zr and crystal bar Zr were very susceptible to the corrosion in 360°C pure water as well as in lithiated water. Zircaloy-4 survived and showed a weight gain of 100mg/dm<sup>2</sup> at 450 days in 360°C pure water. These results are similar to the US testing with the pure Zr materials exhibiting breakaway behavior and Zircaloy-4 showing periodic growth of the oxide. However, the corrosion rate of Zircaloy-4 was increased in lithiated water and the oxide changed to brown and showed the evidence of the partial spallation.

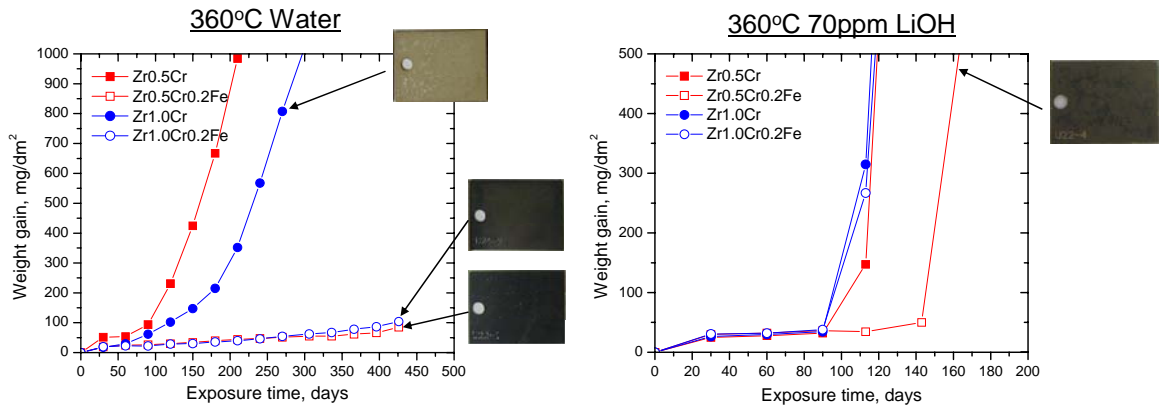
Figure 2.14 shows the corrosion behavior of Zr-Nb alloys in 360°C pure water and in 360°C lithiated water with 70 ppm Li. The corrosion rate was increased with increase of Nb content in Zr-0.2Nb and Zr-0.4Nb which are designed to investigate the solute element effects on the corrosion of Zr alloys. In the Zr-Nb alloys whose Nb content was more than the solubility in alpha-Zr, the corrosion rate was slightly decreased with increase of the Nb content. The oxide was still black and maintained to be adherent even up to 600 days regardless of alloys compositions. Zr-Nb alloys were very susceptible to the breakaway corrosion in 360°C lithiated water. The corrosion rate was accelerated just after 60 days in Zr-0.2Nb and Zr-0.4Nb. However, the time to the breakaway was extended to the longer time when Nb content was more than the solubility limit. The color of the oxide changed to brown but the oxide was not spalled after the breakaway.

Figure 2.15 shows the corrosion behavior of the Zr-Nb-Sn alloys in 360°C water and in 360°C lithiated water. Zr-0.4Sn-0.4Nb showed a lower corrosion rate when compared to Zr-0.4Sn-0.2Nb. However, in the Zr-Nb binary alloys, the Zr-0.2Nb showed a lower corrosion resistance than Zr-0.4Nb. It was thought that the corrosion mechanism of the Sn containing alloys was different from the binary alloys. Moreover, the Sn addition was very beneficial for the corrosion resistance in lithiated water. The time to the breakaway was about three times longer in Sn-containing ternary alloys.

The corrosion resistance of Zr-Sn binary alloys was similar to each other and their corrosion rate was maintained at the relatively lower level before the breakaway, as shown in Figure 2.16. After 280 days, Zr-0.8Sn and Zr-1.2Sn alloys showed the breakaway corrosion behavior. The weight gain increment of Zr-1.2Sn was two times greater than that of Zr-0.8Sn. The color of the oxide was changed to be brown in Zr-1.2Sn. However, the Zr-0.2Sn and Zr-0.4Sn alloys maintained their lower corrosion rate up to 350 days. The Zr-Sn alloys have more corrosion resistance than Zr-Nb alloys in lithiated water. Their corrosion resistance was increased with increase of Sn content in lithiated water except for Zr-1.2Sn.



**Figure 2.8:** Corrosion behavior of US-manufactured Zr-Fe-Cr alloys in 360°C pure water and lithiated water.



**Figure 2.9:** Corrosion behavior of US-manufactured Zr-Cr-Fe alloys in 360°C pure water and lithiated water.

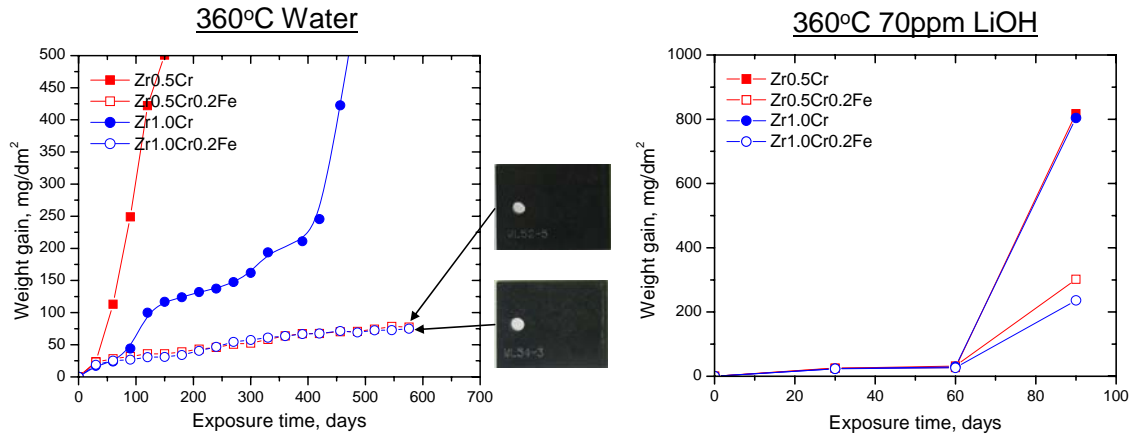


**Figure 2.10:** Corrosion behavior of ROK-manufactured Zr-Cr-Fe alloys in 360°C pure water and lithiated water.

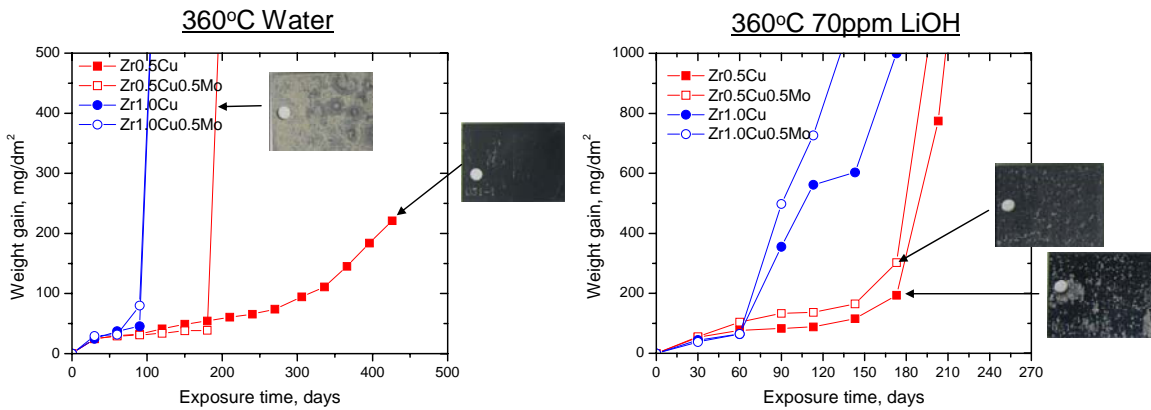


**Figure 2.11:** Corrosion behavior of US-manufactured Zr-Cu-Mo alloys in 360°C pure water and lithiated water.

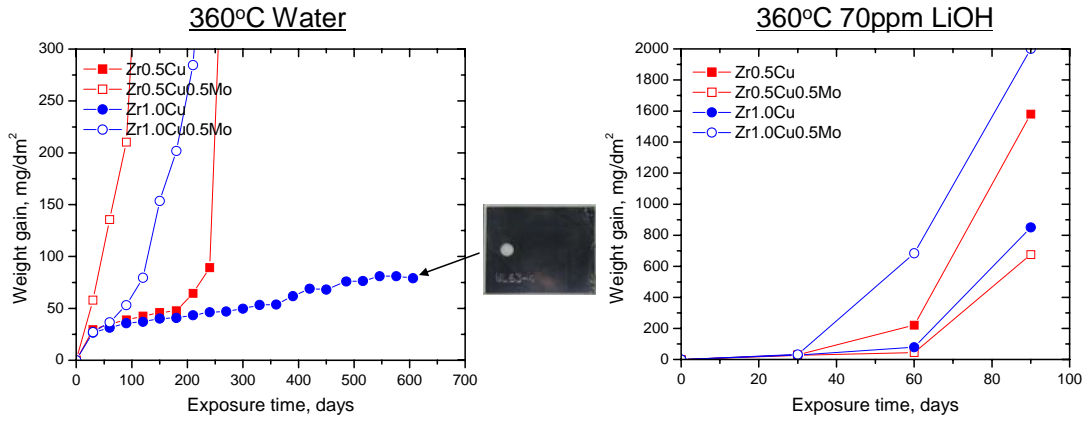


**Figure 2.12:** Corrosion behavior of ROK-manufactured Zr-Cu-Mo alloys in 360°C pure water and lithiated water.

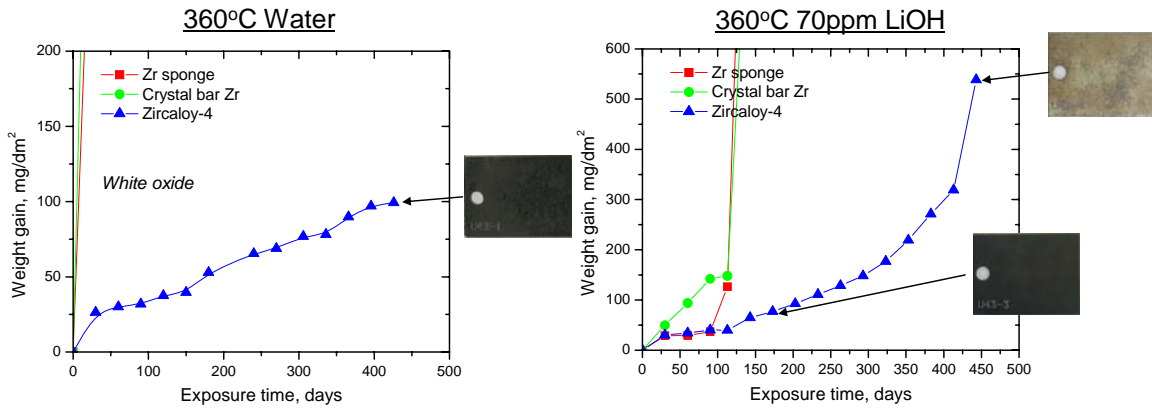


**Figure 2.13:** Corrosion behavior of the reference alloys in 360°C pure water and lithiated water.

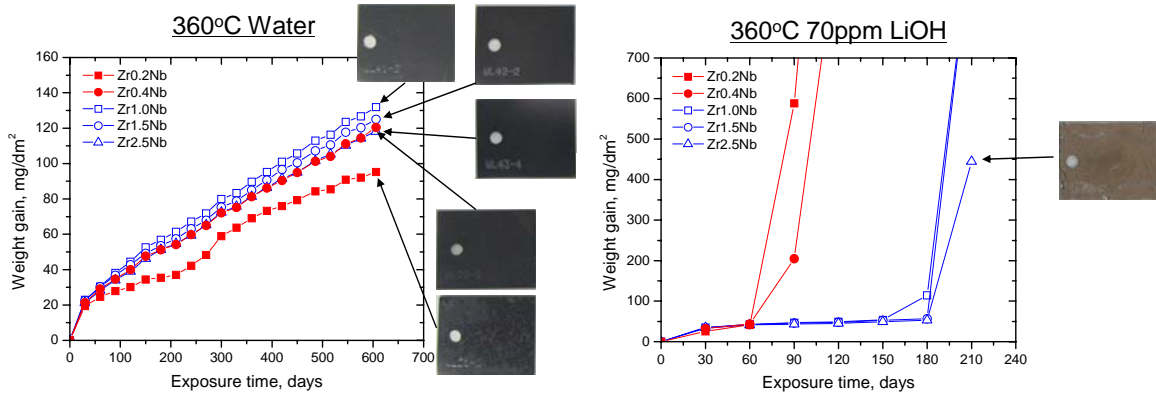


**Figure 2.14:** Corrosion behavior of Zr-Nb alloys in 360°C pure water and lithiated water.

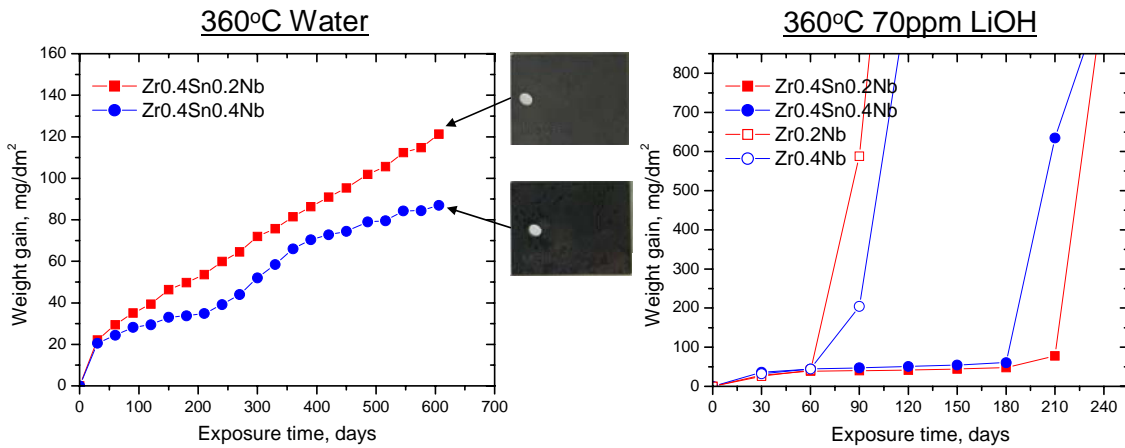


**Figure 2.15:** Corrosion behavior of Zr-Sn-Nb alloys in 360°C pure water and lithiated water.

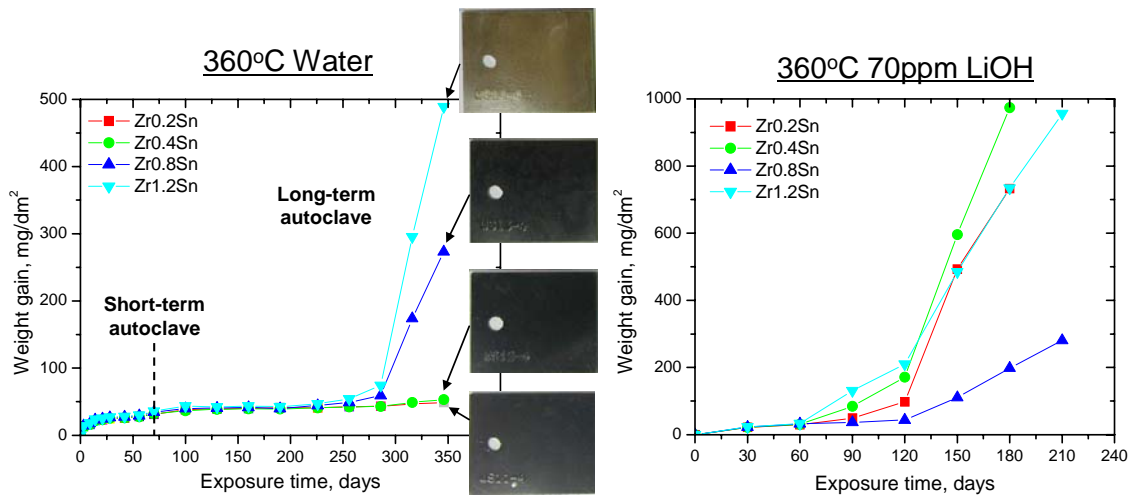


**Figure 2.16:** Corrosion behavior of Zr-Sn alloys in 360°C pure water and lithiated water.